Proceedings of the ASME 2018 International Design Engineering Technical Conferences & Computers and Information in Engineering Conference
IDETC/CIE 2018
August 26-29, 2018, Quebec City, Quebec, Canada

DETC2018-85202

PARADOXICAL CHAOS-LIKE CHATTERING IN THE BOUNCING BALL SYSTEM

Kilian Schindler
Risk Analytics and Optimization Chair
École Polytechnique Fédérale de Lausanne
Switzerland
kilian.schindler@epfl.ch

Remco I. Leine*
Institute for Nonlinear Mechanics
University of Stuttgart
Germany
leine@inm.uni-stuttgart.de

ABSTRACT

This paper reports and investigates paradoxical simulation results of the bouncing ball system. Chaos-like motion of the bouncing ball system with intermittent chattering (Zeno behaviour) is observed in simulations if the relative acceleration of the table exceeds a critical value. However, one can show that this is theoretically impossible. A detailed analysis is given by looking at the backward and forward dynamics of grazing solutions. It is shown in detail that a self-similar structure appears if the relative acceleration of the table exceeds the critical value.

INTRODUCTION

The one-dimensional harmonically excited bouncing ball system (see Fig. 1) has an appealing simplicity allowing for closed form analysis and has an extremely rich dynamic behaviour despite this simplicity, explaining the huge interest in literature for this intriguing problem, e.g. see [1–4] and also [6] in which a high-bounce approximation is made. In previous work [5] on stability properties of the bouncing ball problem, a strange curiosity was encountered. The bouncing ball system was simulated using a standard integration scheme for non-smooth systems (Moreau's timestepping scheme). An erratic oscillatory motion was obtained, which to all appearances looks as a chaotic attractor, Fig. 2. The motion irregularly visits an accumulation point (chattering) after which the ball is in contact with the table for a while and then lifts off again. Two such accumulation points can be seen in Fig. 2. However, such trajectories cannot actually exist. Namely, if the ball comes to rest on the oscillating table after a chattering phase, then it remains in contact with the table up to the next time instant allowing for detachment. The time instant of detachment (or its phase with respect to the excitation period), however, is uniquely defined: it is exactly that time instant for which the table accelerates downward with an acceleration equal to gravity causing the contact force between ball and table to vanish. Hence, at the time instant of detachment the position and velocity of the ball, being those of the table, are known and also the phase of excitation is known, which implies that there is a unique solution after lift-off. The motion evolving from any phase of persistent contact must therefore be identical, irrespectively of how the ball came to rest on the table. As a consequence, if the trajectory after an accumulation point encounters a new accumulation point, this procedure must repeat endlessly, implying that the resulting motion is periodic.

This work, which is based on the MSc. thesis [7], gives an explanation for the contradiction between theory and simulation of the bouncing ball system.

THE IMPACT MAPS OF THE BOUNCING BALL SYSTEM

We consider the one-dimensional bouncing ball system (see Fig. 1) consisting of a rigid ball of mass m bouncing on a vertically moving flat table under the influence of a constant gravitational field g. We denote by $q(t)$ the absolute height of the ball, and by $e(t)$ the absolute vertical position of the kinematic excitation of the table, which is assumed to be harmonic

$$e(t) = -A\sin(\Omega t). \tag{1}$$

*Address all correspondence to this author.

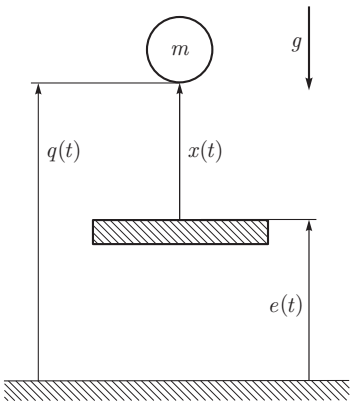

FIGURE 1. The Bouncing Ball System.

The acceleration ratio between the maximum absolute table acceleration and the gravitational acceleration is abbreviated with the dimensionless parameter

$$\kappa := \frac{A\Omega^2}{g} \geq 0. \tag{2}$$

The distance between ball and table will be addressed by $x(t)$ and is non-negative due to the unilateral constraint, i.e.

$$x(t) = q(t) - e(t) \geq 0. \tag{3}$$

Accordingly, between impact events, the relative velocity of the ball with respect to the table is $v(t) = \dot{x}(t) = \dot{q}(t) - \dot{e}(t)$.

The impact process itself is modelled by a strictly dissipative Newton-type impact law with restitution coefficient r,

$$x(t_n) = 0: \quad v^+(t_n) = -r\,v^-(t_n), \tag{4}$$

where t_n is an impact time instant and $v^+(t_n) = \lim_{t \downarrow t_n} v(t)$ and $v^-(t_n) = \lim_{t \uparrow t_n} v(t)$ are the post- and pre-impact velocity, respectively. We consider values of the restitution coefficient $0 < r < 1$. In the following, we will show that the system is completely described by the two parameters κ and r.

We will need to distinguish between four sets of time instants describing different phases of the excitation period, namely

$$\text{lift-off:} \qquad \mathscr{L}_t := \left\{ t \in \mathbb{R} \mid \ddot{e}(t) < -g \right\}, \tag{5}$$

$$\text{sticking:} \qquad \mathscr{S}_t := \left\{ t \in \mathbb{R} \mid \ddot{e}(t) > -g \right\}, \tag{6}$$

$$\text{detachment:} \qquad \mathscr{D}_t := \left\{ t \in \mathbb{R} \mid \ddot{e}(t) = -g \wedge \dddot{e}(t) < 0 \right\}, \tag{7}$$

$$\text{attachment:} \qquad \mathscr{A}_t := \left\{ t \in \mathbb{R} \mid \ddot{e}(t) = -g \wedge \dddot{e}(t) \geq 0 \right\}. \tag{8}$$

In absence of any contact force, the ball will move under the sole influence of gravity, $m\ddot{q}(t) = -mg$. The equations of motion for contact-free time intervals $\mathscr{T}_{CF}$ can therefore be expressed in the states x and v as

$$\left.\begin{aligned} \dot{x}(t) &= v(t) \\ \dot{v}(t) &= -g - A\Omega^2 \sin(\Omega t) \end{aligned}\right\} \quad \forall t \in \mathscr{T}_{CF}. \tag{9}$$

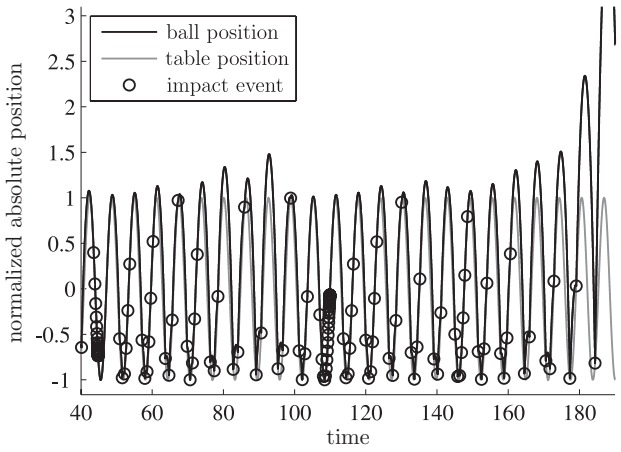

FIGURE 2. Excerpt of a simulation using the timestepping scheme.

In presence of persistent contact (contact during a time lapse), a finite contact force $\lambda(t) \geq 0$ is added to the equation of motion $m\ddot{q}(t) = -mg + \lambda(t)$. Throughout the persistent contact, the contact force $\lambda(t)$ takes precisely the value required to maintain contact between ball and table, $\lambda(t) = mg + mA\Omega^2 \sin(\Omega t)$.

Let $v_n := v^+(t_n)$ denote the post-impact velocity at the n-th impact time instant t_n. Integration of the equations of motion (9) together with $x(t_{n+1}) = x(t_n) = 0$ yields

$$\begin{aligned} 0 = &-\frac{1}{2} g (t_{n+1} - t_n)^2 + (v_n - A\Omega\cos(\Omega t_n))(t_{n+1} - t_n) \\ &+ A(\sin(\Omega t_{n+1}) - \sin(\Omega t_n)), \end{aligned} \tag{10}$$

$$v_{n+1} = rg(t_{n+1} - t_n) - rA\Omega(\cos(\Omega t_{n+1}) - \cos(\Omega t_n)) - rv_n. \tag{11}$$

Given the pair (t_n, v_n), these are two nonlinear implicit equations for the unknowns (t_{n+1}, v_{n+1}).

If $v_n = 0$, then a phase of persistent contact starts, which ends if the contact force λ vanishes. The time t_D, denoting the end of persistent contact, is therefore the first time instant $t_D > t_n$ such that $\lambda(t_D) = mg + mA\Omega^2 \sin(\Omega t_D) = 0$.

In order to improve numerical stability and allow for a dimensionless analysis of the bouncing ball dynamics, we will introduce a new dimensionless impact time instant τ_n given by

$$\tau_n := \frac{\Omega}{2\pi} t_n, \tag{12}$$

such that the resulting dimensionless excitation period equals unity. Furthermore, we introduce a dimensionless post-impact velocity w_n, and a new dimensionless relative distance ξ:

$$w_n := \frac{\Omega}{\pi g} v_n, \qquad \xi(t) := \frac{1}{2} \frac{\Omega^2}{\pi^2 g} x(t). \tag{13}$$

The four sets of time instants describing the different phases of the excitation period can also be translated into their dimension-

less counterparts $\mathscr{L}_\tau$, $\mathscr{S}_\tau$, $\mathscr{D}_\tau$ and $\mathscr{A}_\tau$.

The forward impact map P is the operation that maps a pair of dimensionless impact states (τ_n, w_n) to the next pair of dimensionless impact states (τ_{n+1}, w_{n+1}),

$$P(\tau_n, w_n) := (\tau_{n+1}, w_{n+1}), \qquad P:\ \mathbb{R}\times\mathbb{R}_0^+ \to \mathbb{R}\times\mathbb{R}_0^+. \quad (14)$$

The k-th iterated forward impact map P^k is defined as

$$P^k(\tau_n, w_n) := \underbrace{P\circ P\circ \ldots \circ P(\tau_n, w_n)}_{P \text{ iterated k times}} = (\tau_{n+k}, w_{n+k}). \quad (15)$$

Forward impact map: *Given any arbitrary pair of dimensionless impact states $(\tau_n, w_n) \in \mathbb{R}\times\mathbb{R}_0^+$, $P(\tau_n, w_n) := (\tau_{n+1}, w_{n+1})$ can be computed as follows:*

Flight: If $w_n > 0$, or if $w_n = 0 \wedge \tau_n \in \mathscr{L}_\tau \cup \mathscr{D}_\tau$.

1. *Find the smallest value $\tau_{n+1} > \tau_n$ that fulfils the implicit equation*

$$0 = -(\tau_{n+1}-\tau_n)^2 + (w_n - \frac{\kappa}{\pi}\cos(2\pi\tau_n))(\tau_{n+1}-\tau_n) + \frac{\kappa}{2\pi^2}(\sin(2\pi\tau_{n+1}) - \sin(2\pi\tau_n)). \quad (16)$$

2. *Given τ_n, w_n and τ_{n+1}, evaluate the expression*

$$w_{n+1} = 2r(\tau_{n+1}-\tau_n) - r\frac{\kappa}{\pi}(\cos(2\pi\tau_{n+1}) - \cos(2\pi\tau_n)) - rw_n. \quad (17)$$

Stick: If $w_n = 0 \wedge \tau_n \in \mathscr{S}_\tau \cup \mathscr{A}_\tau$.

1. *Find the smallest element $\tau_D \in \mathscr{D}_\tau$ such that $\tau_n < \tau_D$.*
2. *Then $P(\tau_n, w_n) = P(\tau_D, 0)$.*

The backward impact map P^{-1} is the operation that maps a pair of dimensionless impact states (τ_n, w_n) to the previous pair of dimensionless impact states (τ_{n-1}, w_{n-1}),

$$P^{-1}(\tau_n, w_n) := (\tau_{n-1}, w_{n-1}). \quad (18)$$

The k-th iterated backward impact map P^{-k} is defined as

$$P^{-k}(\tau_n, w_n) := \underbrace{P^{-1}\circ P^{-1}\circ \ldots \circ P^{-1}(\tau_n, w_n)}_{P^{-1} \text{ iterated k times}} = (\tau_{n-k}, w_{n-k}). \quad (19)$$

Backward impact map: *Given any arbitrary pair of dimensionless impact states $(\tau_n, w_n) \in \mathbb{R}\times\mathbb{R}_0^+$, $P^{-1}(\tau_n, w_n) := (\tau_{n-1}, w_{n-1})$ can be computed as follows:*

Flight: If $w_n > 0$, or if $w_n = 0 \wedge \tau_n \in \mathscr{L}_\tau \cup \mathscr{A}_\tau$.

1. *Find the largest value $\tau_{n-1} < \tau_n$ that fulfills the implicit equation*

$$0 = (\tau_n-\tau_{n-1})^2 - (\frac{1}{r}w_n + \frac{\kappa}{\pi}\cos(2\pi\tau_n))(\tau_n-\tau_{n-1}) + \frac{\kappa}{2\pi^2}(\sin(2\pi\tau_n) - \sin(2\pi\tau_{n-1})). \quad (20)$$

2. *Given τ_n, w_n and τ_{n-1}, evaluate the expression*

$$w_{n-1} = 2(\tau_n-\tau_{n-1}) - \frac{\kappa}{\pi}(\cos(2\pi\tau_n) - \cos(2\pi\tau_{n-1})) - \frac{1}{r}w_n. \quad (21)$$

Stick: If $w_n = 0 \wedge \tau_n \in \mathscr{S}_\tau \cup \mathscr{D}_\tau$.

Due to non-uniqueness of trajectories in backward time, it is not possible to find a meaningful backward impact map for this case. For completeness, we arbitrarily define: $P^{-1}(\tau_n, w_n) = (\tau_n, w_n)$.

The forward impact map $P:(\tau_n, w_n) \mapsto (\tau_{n+1}, w_{n+1})$ is discontinuous at grazing points, i.e. at (τ_n, w_n) that are mapped to $(\tau_{n+1}, 0)$. With $B^1 := \{(\tau_n, w_n) = P^{-1}(\tau_{n+1}, 0), \tau_{n+1} \in \mathbb{R}\}$ we denote the set of discontinuity points of P. Similarly, with $F^1 := \{(\tau_n, w_n) = P(\tau_{n-1}, 0), \tau_{n-1} \in \mathbb{R}\}$ we denote the set of discontinuity points of the backward impact map P^{-1}. Furthermore, the N-th iterated forward impact map P^N is discontinuous at $B^k := \{(\tau_n, w_n) = P^{-k}(\tau_{n+k}, 0), \tau_{n+k} \in \mathbb{R}\}$ for all $k \le N$. Similarly, the N-th iterated backward impact map P^{-N} is discontinuous at $F^k := \{(\tau_n, w_n) = P^k(\tau_{n-k}, 0), \tau_{n-k} \in \mathbb{R}\}$ for all $k \le N$.

ACCUMULATION BARRIER

Time intervals of persistent contact between ball and table play a very special role in the dynamics of the bouncing ball system. On the one hand, they are responsible for the loss of uniqueness of trajectories in backward time. On the other hand, in forward time, these phases of persistent contact have the very special effect of gathering infinitely many trajectories prior to releasing all of them at exactly the same detachment time instant τ_D given by $1 + \kappa\sin(\tau_D) = 0$.

Besides the obvious case in which a trajectory starts within a persistent contact phase due to corresponding initial conditions, it is also possible for trajectories to dynamically fall into such phases of persistent contact by means of accumulation points, that is, the occurrence of an infinite number of impacts with ever decreasing post-impact velocities happening within a finite time interval before the ball eventually lies on the table, see Fig. 3.

If the forward impact map approaches an accumulation point, it will not be able to go beyond, because, mapping a given pair of impact states to the next pair and so forth, it will not be able to overcome the infinite number of impact events leading to that accumulation point.

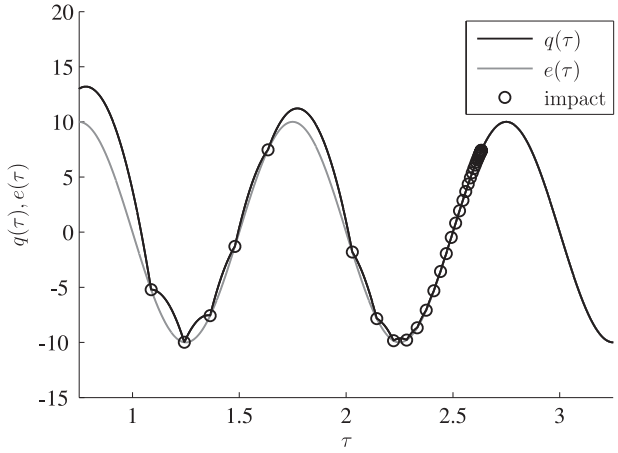

FIGURE 3. Illustration of an accumulation point.

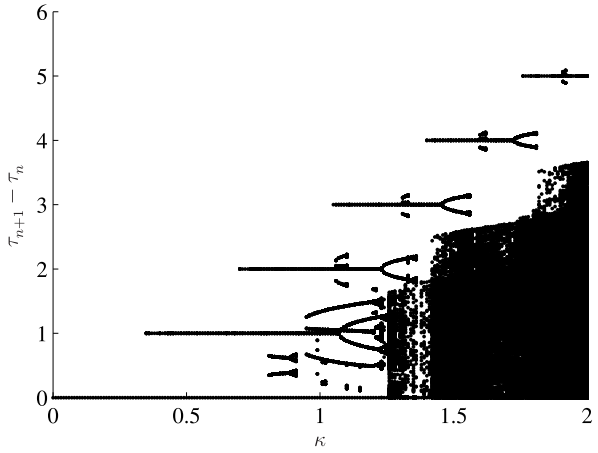

FIGURE 4. Brute force diagram for $n_1 = 1000$ transitive iterations.

BRUTE FORCE DIAGRAMS

A brute force diagram of the bouncing ball system with κ as bifurcation parameter is shown in Fig. 4 for $r = 0.8$. At each value of κ, the system is iterated n_1=1000 times with the forward impact map to allow for transient motion to decay. Subsequently the following $N = 10$ iterations are plotted in the brute force diagram. This is repeated for different initial conditions to find coexisting attractors. The brute force diagram has been constructed again in Fig. 5 using n_2 =10'000 transitive iterations of P.

Besides the dominant dark area in the lower right-hand corner of Fig. 4, the most prominent structures that can be identified in both figures are the five horizontal stripes at the height of integer dimensionless flight times with the cascade of bifurcations at their right ends. These structures belong to periodic solution with no intermediate impacts, that is, the period time of such trajectories corresponds exactly to the flight time of the ball between consecutive impacts. Fig. 6 illustrates an example of a trajectory converging to such a periodic solution. In contrast, periodic solutions with intermediate impacts give rise to groups of curved horizontal stripes, where each stripe is at the height of different, not necessarily integer dimensionless flight times. The period time of such periodic solutions corresponds to the sum of flight times between all impact events belonging to the respective periodic solution, see Fig. 7.

The striking difference between Fig. 4 and Fig. 5 is the almost disappearing dark region in the bottom right corner of Fig. 4, suggesting the existence of a big chaotic attractor in the system. According to Fig. 4, it looks as if chaotic motion is suddenly created as soon as the value of κ exceeds a precise threshold $\hat{\kappa} \approx 1.225$. However, this suggestion cannot be confirmed by Fig. 5, where only very little of the dark region is left. A similar observation has been made in [5]. A possible interpretation is that the big dark region of Fig. 4 is actually only a transient,

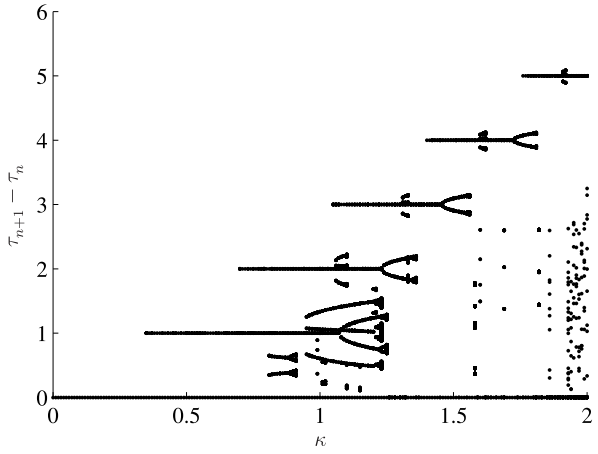

FIGURE 5. Brute force diagram for n_2 =10'000 transitive iterations.

which disappears accordingly if the transient phase of the simulation is chosen long enough. The aim of the present paper is to determine whether anything particular occurs at the moment when κ reaches $\hat{\kappa}$, and based on those findings to give an alternative explanation for this particularity.

A horizontal line at (almost) zero flight time appears both in Fig. 4 and Fig. 5. There are two types of dynamical behavior that can give rise to such an object: either the equilibrium where ball and table already start and then remain in persistent contact for all future times (only possible for $\kappa \leq 1$), or an accumulation point, which the forward impact map cannot overcome, giving rise to chattering (possible for all κ). Almost all points on this line belong to the second category.

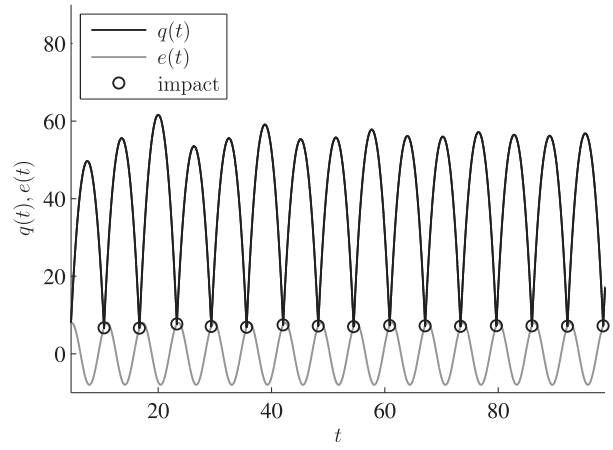

FIGURE 6. A periodic solution without intermediate impacts.

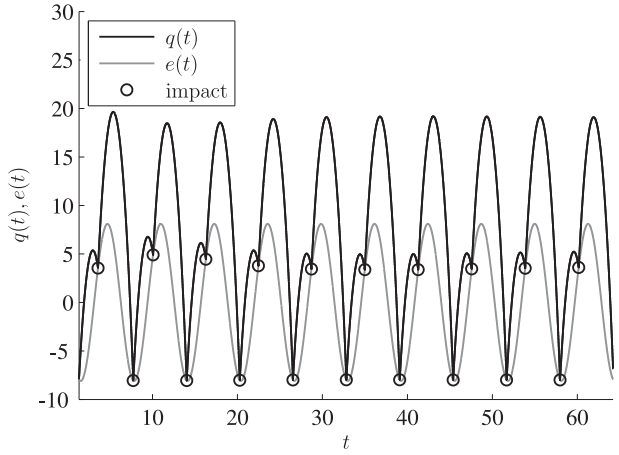

FIGURE 7. A periodic solution with one intermediate impact.

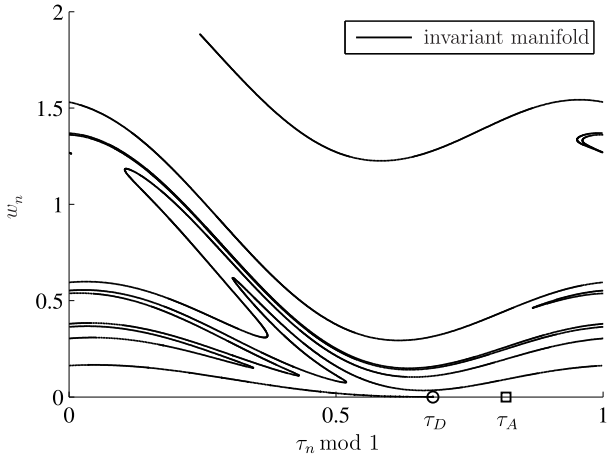

FIGURE 8. Invariant manifold for $r = 0.8$ and $\kappa = 1.1 < \hat{\kappa}$.

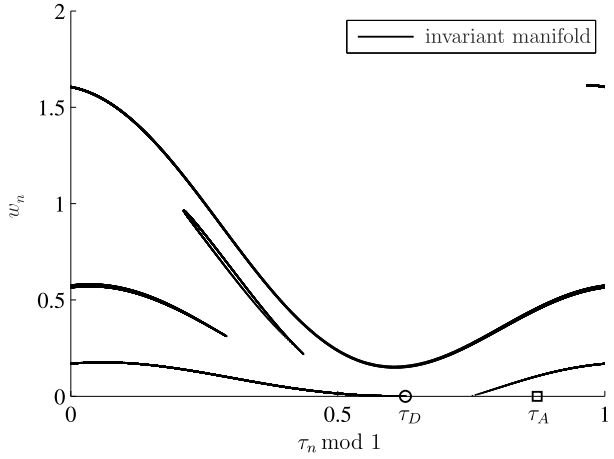

FIGURE 9. Invariant 'manifold' for $r = 0.8$ and $\kappa = 1.4 > \hat{\kappa}$.

ANALYSIS OF CHATTERING MOTION

From now on it will be convenient to consider the phase of the impact events with respect to the excitation period rather than the absolute time at which they occur. Accordingly, we denote the (unique) detachment phase by $\tau_D = \tau_n \mod 1$ for any $\tau_n \in \mathscr{D}_\tau$ and the (unique) attachment phase by $\tau_A = \tau_n \mod 1$ for any $\tau_n \in \mathscr{A}_\tau$. Our analysis of the chattering motion of the bouncing ball system follows closely the procedure adopted by Budd & Dux in [8] for the analysis of chattering phenomena in impact oscillators. Consider $\lambda_i \in \mathbb{R}^+$, where $\lambda_i < \frac{2}{3}$. Then, for any parabola parameterized by λ_i with minimum in $(\tau_D, 0)$

$$\begin{aligned}\mathscr{P}_{\lambda_i} := \big\{ (\tau_n, w_n) \in \mathbb{R} \times \mathbb{R}_0^+ \mid \\ w_n = -2\pi\kappa\cos(2\pi\tau_D)\,\lambda_i\,(\tau_D - \tau_n)^2,\ \tau_n < \tau_D \big\},\end{aligned} \tag{22}$$

assuming $\tau_D - \tau_n \ll 1$ and $0 < w_n \ll 1$ to be sufficiently small, it holds that

$$P(\mathscr{P}_{\lambda_i}) = \mathscr{P}_{\lambda_{i+1}}, \tag{23}$$

where the λ_{i+1} is a function $f : (0, \frac{2}{3}) \to \mathbb{R}^+$ of λ_i:

$$\lambda_{i+1} = f(\lambda_i) = -r\left(1 - \frac{1-\lambda_i}{(1-\Theta(\lambda_i))^2}\right), \tag{24}$$

$$\Theta(\lambda_i) := \frac{3}{2} - \sqrt{\left(\frac{3}{2}\right)^2 - 3\lambda_i}. \tag{25}$$

For small values of $\tau_D - \tau_n$ and w_n, the points of a given parabola $\mathscr{P}_{\lambda_i}$ are mapped onto another parabola $\mathscr{P}_{\lambda_{i+1}}$ such that $\lambda_{i+1} = f(\lambda_i)$. Thus, close to $(\tau_D, 0)$ the effect of the forward impact map P can be analyzed by means of the one-dimensional map $f(\lambda)$,

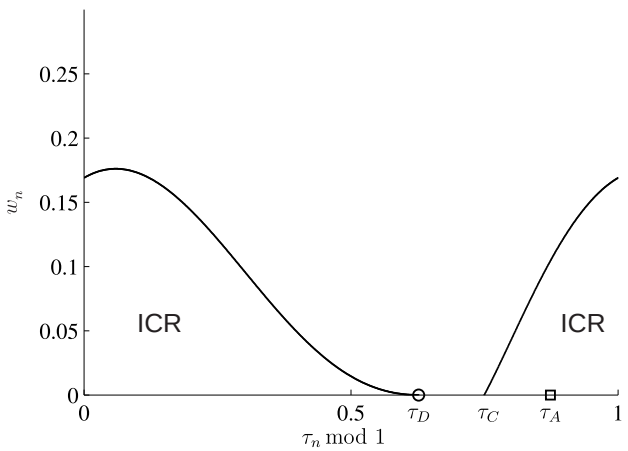

FIGURE 10. Invariant chattering region for $r = 0.8$, $\kappa = 1.4 > \hat{\kappa}$.

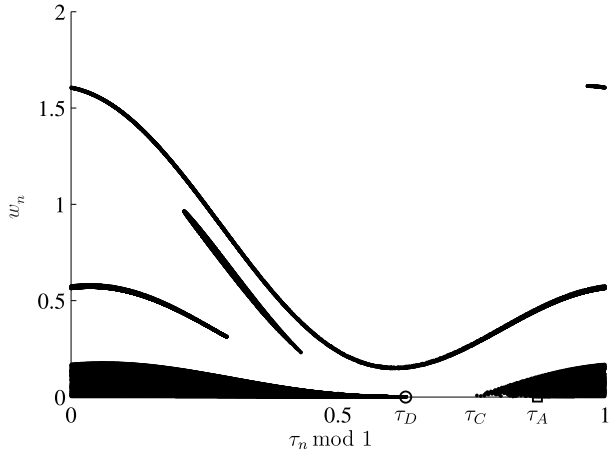

FIGURE 11. First two backward iterates of the invariant chattering region for $r = 0.8$, $\kappa = 1.4 > \hat{\kappa}$.

which has a unique fixed point $\lambda_\infty = f(\lambda_\infty)$ within the interval $(0, \frac{2}{3})$. The fixed point λ_∞ corresponds to an invariant parabola $\mathscr{P}_\infty$, which is indeed invariant in the neighbourhood of $(\tau_D, 0)$.

The invariant parabola $\mathscr{P}_\infty$ forms the beginning of an invariant manifold starting at $(\tau_D, 0)$. Using the tracking algorithm described in [9], one can track this invariant manifold by means of the backward impact map. Fig. 8 depicts the tracking result for $r = 0.8$ and $\kappa = 1.1 < \hat{\kappa}$. Fig. 9 illustrates the result for the case $r = 0.8$ and $\kappa = 1.4 > \hat{\kappa}$, which has been obtained with a slightly extended algorithm tracking discontinuities. The tracking algorithm was stopped on purpose once the generated image provided reasonable evidence of the invariant manifold's structure. Two conclusions can be drawn from these figures:

1. For $\kappa < \hat{\kappa}$, the invariant manifold is a continuous open curve. For $\kappa \geq \hat{\kappa}$, the invariant 'manifold' is a non-continuous, piecewise closed curve, which clearly divides the impact space into separate regions.
2. For increasing values of κ, the transition between these two topologies is characterized by the piece-wise closure and disconnection of the manifold. Accordingly, in the opposite direction the same transition is characterized by the aperture and mutual connection of the 'manifold's pieces'.

For $\kappa \geq \hat{\kappa}$, the invariant 'manifold' divides the impact space into well-defined separate regions, and from this fact we can take further advantage. Consider only $\kappa \geq \hat{\kappa}$. Then, the *invariant chattering region* (ICR) is defined as the set of all impact states (τ_n, w_n) enclosed by the zero velocity line and that part of the invariant 'manifold' situated between $(\tau_D, 0)$ and its first intersection $(\tau_C, 0)$ with the zero velocity line, see Fig. 10. Any trajectory evolving from the ICR directly experiences chattering in its immediate future, i.e. within the same period of excitation. This immediately follows from the fact that $0 < f(\lambda) < \lambda$ for $0 < \lambda < \lambda_\infty$, which implies that $f(\lambda)^k \to 0$ for $k \to \infty$.

Besides trajectories evolving directly from impact states within the ICR, also trajectories evolving from impact states within any pre-iterate of the ICR will experience chattering at some point. An illustration of the ICR and its first two backward iterates for the case $r = 0.8$ and $\kappa = 1.4$ is given in Fig. 11. Notice in particular that the pre-iterates of the ICR correspond exactly to the impact states enclosed by the various pieces of the previously computed invariant 'manifold' in Fig. 9. Accordingly, the invariant 'manifold' itself consists precisely of the several pre-iterates of the invariant chattering region border, a fact which facilitates their computation.

An important advantage of the invariant chattering region consists in its applicability to determine the motion evolving after an accumulation point. The behaviour of trajectories evolving from an accumulation point is completely described by the dynamics of the detachment point $(\tau_D, 0)$. If the trajectory of the detachment point is attracted towards a periodic or chaotic attractor, then all chattering trajectories will be attracted as well. Conversely, if the trajectory of the detachment point eventually falls into an accumulation point, so will all chattering trajectories, which implies the existence of a periodic solution with accumulation points. Now, to determine whether the trajectory of the detachment point experiences chattering, we can make use of the previously defined invariant chattering region. If $\kappa \geq \hat{\kappa}$ and $P(\tau_D, 0)$ is in the ICR or some pre-iterate of the ICR, then all trajectories that experience chattering once will, from then onwards, experience chattering on a periodic basis. The period time of this resulting periodic solution corresponds exactly to the number of excitation periods the trajectory evolving from $(\tau_D, 0)$ requires to re-enter the ICR. We define the *return number R* as the number of impacts experienced by the trajectory evolving from $(\tau_D, 0)$

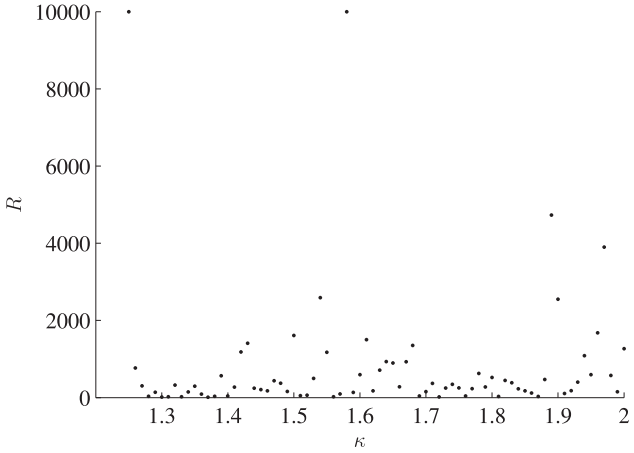

FIGURE 12. Return number R for $\kappa \in [1.25, 2]$.

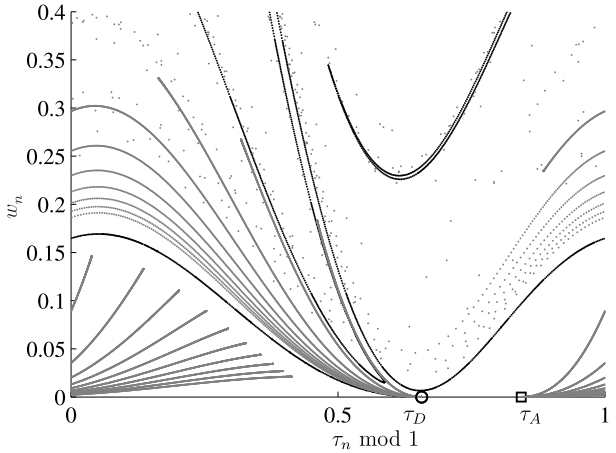

FIGURE 13. Discontinuities of impact maps in the subcritical regime (F^k and B^k for $k = 1, 2, \ldots, 10$ at $\kappa = 1.2 < \hat{\kappa}$ and $r = 0.8$).

prior to entering the ICR. Fig. 12 illustrates the return number for $r = 0.8$ under variation of $\kappa \geq \hat{\kappa}$ up to a maximal return number of 10'000. As can be seen, although there are major fluctuations, a vast majority of κ-values yields finite return numbers R. This indicates that for most values of κ the trajectory evolving from an accumulation point returns to the invariant chattering region after R impacts. In other words, for most values of the acceleration ratio κ, accumulation points give rise to periodic solutions with repeated chattering.

EXPLANATION OF SUDDEN CHAOS-LIKE BEHAVIOR

As observed in the previous sections, when κ exceeds the threshold $\hat{\kappa}$ the behavior of the bouncing ball system changes suddenly. Considering the trajectories evolving from several initial conditions after a transient phase of 1000 impact events, it appears as if the system behaves in a chaotic manner (see Fig. 4). Considering the same trajectories after a longer transient phase of 10'000 impact events, however, shows that most of this chaos-like behavior has disappeared (see Fig. 5). In this section, give an explanation for this conspicuous phenomenon by looking at the global behavior of the discontinuity sets B^k and F^k. Unfortunately, we will increasingly need to rely on numerical results and be careful when drawing conclusions from them.

For $\kappa = 1.2 < \hat{\kappa}$ and $r = 0.8$, Fig. 13 illustrates the numerically computed discontinuity sets F^k (grey, emanating from $(\tau_A, 0)$) and B^k (grey, emanating from $(\tau_D, 0)$) for $k = 1, 2, \ldots, 10$ together with an excerpt of the corresponding invariant manifold (black) computed by means of the aforementioned tracking algorithm. We observe that the two families of sets do not intersect. This behavior can also be confirmed for increasing values of $k > 10$, and the overall topology remains unaltered under variation of the parameter κ in the range $1 < \kappa < \hat{\kappa}$. The k-times forward mapped detachment point $P^k(\tau_D, 0)$ corresponds for each k to the right end of the set F^k. Notice, moreover, that Fig. 13 illustrates how the detachment point trajectory experiences chattering immediately after lift-off.

As the value of κ approaches the threshold $\hat{\kappa}$, the right ends of the sets F^k approach the invariant manifold, which represents the accumulation border of the sets B^k. Precisely at the threshold $\kappa = \hat{\kappa}$, the right ends of F^k come to lie on the invariant manifold. And once $\kappa > \hat{\kappa}$, the sets F^k intersect the invariant manifold, and hence infinitely many sets B^k. An illustration of the latter situation for $\kappa = 1.25 > \hat{\kappa}$ and $r = 0.8$ is depicted in Fig. 14.

The intersections of F^k with B^k lead to important implications for the detachment point trajectory. As long as $\kappa < \hat{\kappa}$, the trajectory evolving from the detachment point falls directly into an accumulation point within the same period of excitation during which it lifted off. Precisely at $\kappa = \hat{\kappa}$ this is still the case, however, the accumulation point is such that there is actually no phase of persistent contact between ball and table any more. Because the forward iterates $P^k(\tau_D, 0)$ of the detachment point lie precisely on the invariant manifold emanating from the latter, the time instant at which the infinite series of impact events terminates corresponds exactly to the detachment time instant itself. As a consequence, the motion starts over again without ball and table having actually been in persistent contact during a non-zero time lapse. Once $\kappa > \hat{\kappa}$, the detachment point trajectory becomes more complicated. As can be seen from Fig. 14, if the value of κ exceeds $\hat{\kappa}$, the series of forward iterates $P^k(\tau_D, 0)$ escapes the previously experienced accumulation, opening the possibility for a completely different type of motion. In other words, the chattering dynamics of the system is interrupted before the ball can come to rest on the table. We know from the analysis of the return number R that for most values of $\kappa > \hat{\kappa}$ the detachment

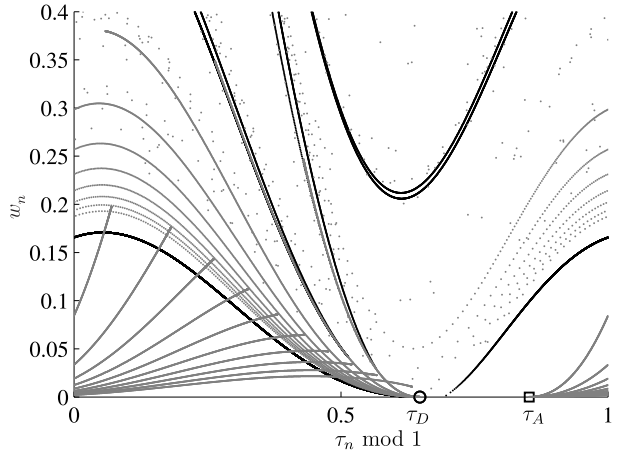

FIGURE 14. Discontinuities of impact maps in the supercritical regime (F^k and B^k for $k = 1,2,\ldots,10$ at $\kappa = 1.25 > \hat{\kappa}$ and $r = 0.8$).

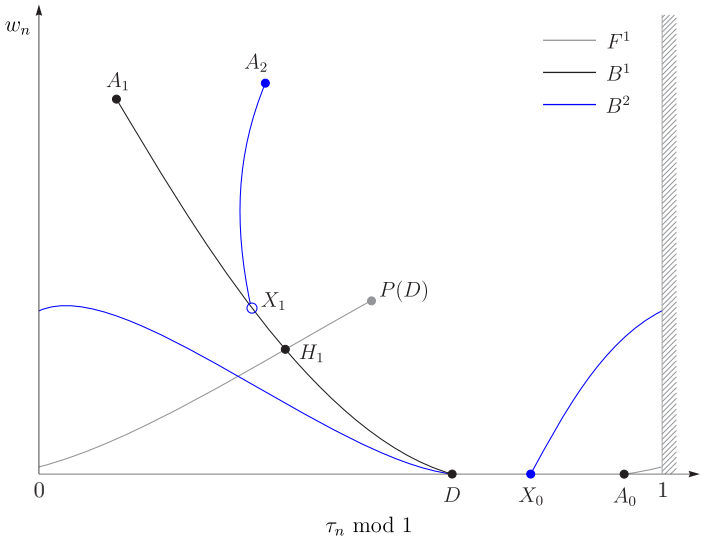

FIGURE 15. Topology of B^1 and B^2 for X_1 above H_1.

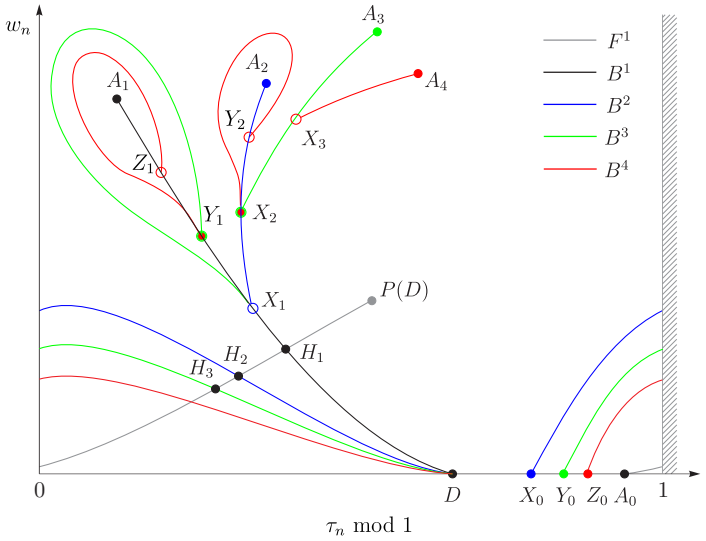

FIGURE 16. Topology of B^1, B^2, B^3 and B^4 for X_1 above H_1.

point trajectory will eventually experience chattering again. Alternatively, it could however also be attracted towards a periodic solution or a chaotic attractor without chattering and therefore having no finite return number R.

These insights confirm the previous observations. However, they are insufficient for a sound explanation of the sudden chaos-like behavior observed in Fig. 4 for $\kappa > \hat{\kappa}$. A better explanation for the sudden apparently chaotic behavior of the bouncing ball system can be found by an in-depth analysis of the topology resulting from the infinitely many intersections between the discontinuity sets F^k and B^k in the supercritical case $\kappa > \hat{\kappa}$ (Fig. 14). We will argue that these intersections give rise to an infinitely fine self-similar structure, which can potentially explain extreme sensitivity on initial conditions in certain regions of the state space.

To start with, consider Fig. 15 illustrating the implication an intersection point H_1 between F^1 and B^1 has for the topological structure of B^2. The set B^1 is the set of all impact states that will be mapped to the zero velocity line by one application of the forward impact map P. The trajectories evolving from impact states in B^1 are hence about to experience a grazing impact. The set F^1 is the once forward mapped zero velocity line, that is, the set of impact states directly succeeding grazing impacts. Moreover, besides the discontinuity induced by non-uniqueness of solutions in backward time, F^1 is the only discontinuity set of the backward impact map P^{-1}.

The existence of an intersection point H_1 between F^1 and B^1 implies two facts about the topology of $B^2 = P^{-1}(B^1)$:

1. The set B^2 must contain a point $X_0 = P^{-1}(H_1)$ on the zero velocity line.
2. The set B^2 consists of two disconnected parts:
   (a) One part connecting the detachment point $D := (\tau_D, 0)$ to the zero velocity line point X_0.
   (b) The other part beginning immediately above $X_1 := P^{-1}(X_0) \in B^1$ and ending at $A_2 := P^{-1}(A_1) \in B^2$, where $A_1 := P^{-1}(A_0) \in B^1$ and $A_0 := (\tau_A, 0)$.

The first assertion stems from the fact that $P^{-1}(F^1)$ corresponds to the zero velocity line according to the definition of the set F^1. Hence, if a point of B^1 is also a point of F^1, then $B^2 = P^{-1}(B^1)$ must contain a point $X_0 = P^{-1}(H_1)$ on the zero velocity line.

The second assertion is more complicated to see. From F^1 being the discontinuity set of the backward impact map P^{-1}, it is clear that if F^1 intersects B^1, then $B^2 = P^{-1}(B^1)$ must be dis-

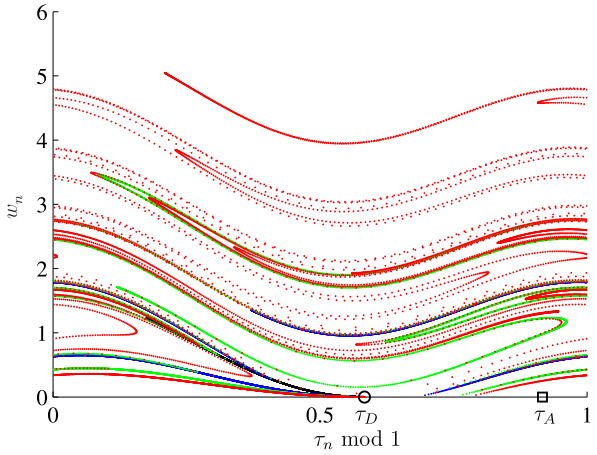

FIGURE 17. Numerically obtained topology of B^1, B^2, B^3 and B^4 for $\kappa = 2$ and $r = 0.8$. Colors have the same meaning as in Fig. 15 and 16.

connected at some point, and hence composed of two continuous pieces. One of these pieces stems from the part of B^1 between D up to and including H_1. The other one results from the part of B^1 between A_1 up to but excluding H_1. Considering the facts that $P^{-1}(D) = D$, $P^{-1}(H_1) = X_0$ and $P^{-1}(A_1) = A_2$, it is clear that one of the two disconnected pieces of B^2 must connect D and X_0, while the other one connects A_2 with the backward map of the point on B^1 immediately above H_1.

The only aspect that remains to be explained is why the backward map of this point on B^1 immediately above H_1 lies exactly above $X_1 = P^{-1}(X_0)$. Recall that F^1 is the set of all impact states that have just experienced a grazing impact. The impact states immediately above F^1, and in particular the point on B^1 immediately above H_1, correspond hence to trajectories that have just flown by because at the previous impact event they had slightly too much post-impact velocity to still experience grazing. The backward map of these points must therefore be the set of impact states that are about to fly by because of too high post-impact velocity. Recalling the fact that B^1 represents the set of all impact states giving rise to trajectories that are about to graze, it is clear that the latter set must be situated immediately above B^1. The fact that, among all possible impact states immediately above B^1, this second component of B^2 begins precisely above $X_1 = P^{-1}(X_0)$ results from the continuity of $B^1 = P(B^2) = P(\textit{first part of } B^2) \cup P(\textit{second part of } B^2)$. Having the second part of B^2 beginning immediately above $X_1 = P^{-1}(X_0)$ is precisely the condition required to guarantee this continuous connection.

Fig. 16 depicts the topology of B^3 and B^4 in addition to the topology shown in Fig. 15. Similarly to our consideration of the different components of B^1 when deriving the topological structure of B^2, we now need to consider the different components of B^2 to infer the topological structure of $B^3 = P^{-1}(B^2)$. From a backward impact map point of view, B^2 consists of three continuously mapped components. A first component from the detachment point D up to and including the first intersection point H_2 between B^2 and F^1. A second one beginning at, but excluding, the intersection point H_2 continuing up to and including the point X_0. And a third component beginning at, but excluding, the point X_1 continuing up to and including the point A_2. Each of these components of B^2 gives rise to a different continuous component of B^3. In the same way, backward mapping the four components of B^3 results in the four components of B^4. Iterating this backward impact mapping mechanism thus gives rise to a self-similar leaves-like structure, which becomes increasingly fine with every additional set B^k as $k \to \infty$.

Although the self-similar topology was derived by means of an example in which B^1 and F^1 intersect, the underlying reasoning remains valid for any supercritical value of κ. As illustrated at the beginning of this section, as soon as $\kappa > \hat{\kappa}$, the right ends of the sets F^k cross the invariant manifold, which is the accumulation curve of the sets B^k, and infinitely many intersections are created between these two set families. As a consequence, if $\kappa > \hat{\kappa}$, there will always exist a finite $N \in \mathbb{N}$ such that B^N and F^N intersect. The assertions made about the topology of the discontinuity sets B^1, B^2, B^3 and B^4 apply then directly to the sets B^N, B^{N+1}, B^{N+2} and B^{N+3} respectively, and the self-similar topology for the supercritical case is valid without loss of generality.

Another aspect that has not been mentioned yet, but which is important for the further argument, is the fact that the backward iterates of the invariant chattering region (Fig. 11) constitute the center of the discontinuity 'leaves'. Notice for example that in Fig. 16, the upper end A_1 of B^1 is enclosed by an outer 'B^3-leaf' (green) connecting Y_1 with X_1, and an inner 'B^4-leaf' (red) connecting Z_1 with Y_1. If we continued to backward iterate the discontinuity sets, the upper end A_1 of B^1, but also the upper end A_k of any other B^k, would become surrounded by an increasing number of such 'leaves'. As in the proximity of the detachment point $(\tau_D, 0)$, it turns out that these 'leaves', which are actually parts of some discontinuity set B^k, accumulate towards the invariant manifold. Recall that in the supercritical case the invariant manifold is composed of many piece-wise continuous closed portions enclosing the pre-iterates of the invariant chattering region. Since A_0 belongs to the invariant chattering region, it follows that the piece-wise closed portions of the invariant manifold must enclose a finite region of the impact space around the points A_k, and that these finite regions are hence pre-iterates of the invariant chattering region. In summary, every 'leaf' consists of infinitely many discontinuity sets B^k surrounding the respective A_k and accumulating towards a respective portion of the invariant manifold enclosing a finite region of the impact space, which hence constitutes the centre of the 'leaf'. These finite regions of the impact space are moreover precisely the backward iterates of the invariant chattering region. It is clear that these assertions

have no mathematical rigor. However, they capture what can be observed from all numerical computations we conducted.

Having clarified the general validity of the self-similar leaves-like structure and the fact that at the center of each leaf there is a finite region of the impact space corresponding to a pre-iterate of the invariant chattering region, it is clear that as soon as κ exceeds $\hat{\kappa}$, the topological structure of the impact space becomes infinitely fine and interweaved. The for $\kappa \leq \hat{\kappa}$ well separated discontinuity sets B^k form now an infinitely intricated self-similar structure, which is in addition extremely stretched along the impact space. As can be seen from B^1, B^2, B^3 and B^4 computed for $\kappa = 2$ and $r = 0.8$ in Fig. 17, this gives rise to regions of the impact space where very small perturbations can result in substantially different trajectory evolutions.

Now, how can this insight be used to explain the occurrence of apparently chaotic trajectories with repeated accumulation points? Imagine that some parts of the trajectory corresponding to a periodic solution with repeated accumulation points lie within one of the regions of the impact space that are highly sensitive to perturbations. When passing through these sensitive regions, due to numerical integration errors, it is possible that the actually periodic trajectory changes its course unexpectedly. For instance, it might follow an adjacent chaotic orbit and return to the periodic one some time later due to a new passage through the same or another region of high sensitivity. If this hypothesis proves correct, it would be a reasonable explanation for apparently chaotic trajectories with repeated accumulation points.

The same reasoning can also explain the sudden chaos-like behavior in Fig. 4 and its almost complete disappearance in Fig. 5. As soon as κ exceeds $\hat{\kappa}$, due to the infinitely fine structure of the state space, trajectories do not necessarily converge to their actual limit sets in a direct manner, but rather change back and forth between the regions of attraction of different limit sets, which can give the impression of chaotic behavior. Moreover, the longer one waits, the more likely it becomes that an arbitrary trajectory incidentally enters the invariant chattering region or one of its very thin and stretched pre-iterates. If this happens, the corresponding trajectory will experience chattering and the forward impact map will not be able to overcome the resulting accumulation point. As a consequence, the originally erratic trajectory will appear near the zero velocity line in the brute force diagram, which is a reasonable explanation for the almost complete disappearance of the chaos-like behavior in Fig. 5.

CONCLUSION

We have given an explanation both for the sudden chaos-like behavior observed in brute force diagrams and for a series of numerical simulation results indicating the existence of irregular trajectories with repeated chattering for $\kappa > \hat{\kappa}$. The latter is a theoretically impossible occurrence as for any given $\kappa > 1$ the ball always lifts off at precisely the same position and with precisely the same velocity, implying that any trajectory with repeated chattering should be periodic due to repeating identical initial conditions. The backbone of our argument is an in-depth analysis of the discontinuities induced by grazing impacts in both the forward and backward impact maps of the bouncing ball system. In particular, we were able to see that these discontinuities intersect infinitely many times and create a self-similar, very interweaved and extremely stretched topological structure as soon as the value of κ exceeds the threshold $\hat{\kappa}$. To explain the two above stated observations, one can imagine that small (finite) disturbances may deviate the respective trajectory from its theoretical evolution and make it dynamically switch between different regions of attraction, resulting in chaos-like behavior or, for instance, irregular motion with repeated chattering. It remains to be investigated if these self-similar structures have a fractal dimension, which would imply fractal boundaries between the regions of attraction of different limit sets.

The practical relevance of these findings consists in the fact that perturbations, caused by numerical errors in simulations, are equally present in the real physical system in form of model inaccuracies and actual unavoidable disturbances. Finally, the results of this paper are strong indications pointing towards a fractalization-like dynamical mechanism interfering with the stability properties of several motions of the bouncing ball system.

REFERENCES

[1] Barroso, J. J., Carneiro, M. V., and Macau, E. E., 2009. "Bouncing ball problem: stability of the periodic modes". *Physical Review E,* ***79***(2), p. 026206.

[2] Giusepponi, S., and Marchesoni, F., 2003. "The chattering dynamics of an ideal bouncing ball". *EPL,* ***64***(1), pp. 36–42.

[3] Luck, J., and Mehta, A., 1993. "Bouncing ball with a finite restitution: chattering, locking, and chaos". *Physical Review E,* ***48***(5), p. 3988.

[4] Vogel, S., and Linz, S. J., 2011. "Regular and chaotic dynamics in bouncing ball models". *IJBC,* ***21***(3), pp. 869–884.

[5] Leine, R. I., and Heimsch, T. F., 2012. "Global uniform symptotic attractive stability of the non-autonomous bouncing ball system". *Physica D: Nonlinear Phenomena,* ***241***(22), pp. 2029 – 2041.

[6] Holmes, P., 1982. "The dynamics of a repeated impacts with a sinusoidally vibrating table". *J. Sound Vibr.,* ***84***(2), pp. 173–189.

[7] Schindler, K., 2013. "Chattering dynamics and related nonlinear motion in the bouncing ball system". Master's thesis, ETH Zurich.

[8] Budd, C., and Dux, F., 1994. "Chattering and related behaviour in impact oscillators". *Phil. Trans. Royal Soc. A,* ***347***(1683), pp. 365–389.

[9] Parker, T. S., and Chua, L. O., 1989. *Practical numerical algorithms for chaotic systems*. Springer New York.